

Behavioral/Systems/Cognitive

Receptive Field Properties of the Macaque Second Somatosensory Cortex: Nonlinear Mechanisms Underlying the Representation of Orientation Within a Finger Pad

Pramodsinh H. Thakur,^{1,3} Paul J. Fitzgerald,^{1,2} John W. Lane,¹ and Steven S. Hsiao^{1,2,3}¹Zanvyl Krieger Mind/Brain Institute, ²Departments of Neuroscience, and ³Biomedical Engineering, The Johns Hopkins University, Baltimore, Maryland 21218

AQ: A We investigate the position invariant receptive field properties of neurons in the macaque second somatosensory (SII) cortical region. Previously we reported that many SII region neurons show orientation tuning in the center of multiple finger pads of the hand and further that the tuning is similar on different pads, which can be interpreted as position invariance. Here we study the receptive field properties of a single finger pad for a subset ($n = 61$) of those 928 neurons, using a motorized oriented bar that we positioned at multiple locations across the pad. We calculate both vector fields and linear receptive fields of the finger pad to characterize the receptive field properties that give rise to the tuning, and we perform an additional regression analysis to quantify linearity, invariance, or both in individual neurons. We show that orientation tuning of SII region neurons is based on a variety of mechanisms. For some neurons, the tuning is explained by simple excitatory regions, simple inhibitory regions, or some combination of these structures. However, a large fraction of the neurons ($n = 20$ of 61, 33%) show position invariance that is not explained well by their linear receptive fields. Finding invariance within a finger pad, coupled with the previous result of similar tuning on different pads, indicates that some SII region neurons may exhibit similar tuning throughout large regions of the hand. We hypothesize that invariant neurons play an important role in tactile form recognition.

Key words: somatosensory cortex; tactile; SII; orientation; receptive field; vector field

Introduction

Fn1 A hallmark of generalized object recognition in vision and touch is the ability to recognize objects independent of where they are located in space or how they are grasped manually. In both systems, the process begins with the activation of peripheral afferents in the eye and hand that encode an initial isomorphic representation of the object. At this level of processing, the neural responses are linear, with individual afferents providing information about the local intensity of stimuli on the retina or the skin. One function of the sensory systems is to transform these initial representations into a form suitable for memory and perception (Phillips et al., 1988), and as such the final representation on which perception is based depends on neurons that respond to features of the stimuli independent of the location of the object (Rolls, 1994; Logothetis et al., 1995; Wallis and Rolls, 1997; Riesenhuber and Poggio, 2002), i.e., extraction of features in a position invariant manner. A transformation from a position variant to a position invariant representation must depend on nonlinear mechanisms (Brincat and Connor, 2004).

Position invariant responses have been reported in a number of visual cortical areas, including primary visual cortex V1

(Hubel and Wiesel, 1968; Thorell et al., 1984), extrastriate visual area V4 (Gallant et al., 1996; Pasupathy and Connor, 1999), inferotemporal cortex IT (Desimone et al., 1984; Sary et al., 1993; Tovee et al., 1994; Ito et al., 1995; Brincat and Connor, 2004; Hung et al., 2005; Quiroga et al., 2005), and medial superior temporal area MST (Graziano et al., 1994). In the somatosensory system, there are only two reports of position invariant responses. In the first, Hyvärinen and Poranen (1978) found a few area 2 neurons that signaled the orientation of a bar independent of where it was presented on the hand. In the second, Fitzgerald et al. (2006a) found many neurons in the second somatosensory (SII) region that had multiple orientation tuned finger pads, and, for those neurons when the bar was indented in the center of their pads, the preferred orientation tended to be highly similar. In the current study, we investigated whether the responses were position invariant at different locations within a single pad and studied in more detail a subset ($n = 61$) of the 928 neurons that were reported in the studies by Fitzgerald et al. (2004, 2006a,b). We repeatedly indented a motorized oriented bar (eight orientations, 22.5° increments) at nine positions per orientation into a single tuned distal finger pad (see Fig. 1a). The aim was to study position invariance as well as determine the degree to which SII region neural responses can be explained by linear mechanisms. We examined orientation tuning for position invariance because oriented edges play a crucial role in the tactile perception of object shape (Johnson and Phillips, 1981; Johansson et al., 1982; Wheat and Goodwin, 2001). This is the fourth in a series of studies about the SII region.

AQ: B

Received Sept. 13, 2006; revised Oct. 31, 2006; accepted Nov. 21, 2006.

This work was supported by National Institutes of Health Grant NS34086.

Correspondence should be addressed to Dr. Steven Hsiao, Zanvyl Krieger Mind/Brain Institute, Johns Hopkins University, 338 Krieger Hall, 3400 North Charles Street, Baltimore, MD 21218. E-mail: steven.hsiao@jhui.edu.

DOI:10.1523/JNEUROSCI.3990-06.2006

Copyright © 2006 Society for Neuroscience 0270-6474/06/2613567-09\$15.00/0

Materials and Methods

Recording methods. For a detailed description of the recording methods and an illustration of the stimulator that was used to indent the bar into the skin, see Fitzgerald et al. (2004). Briefly, we recorded from single neurons in the SII hand region of four hemispheres of two rhesus monkeys (*Macaca mulatta*). Thirty-five to 45 d were spent recording in each hemisphere. Single-neuron data were collected while the monkeys performed a visual detection task that maintained them in a nearly constant state of alertness. The monkeys were trained to allow their hands to be restrained during the single-unit recording sessions, because this allowed for accurate and repeatable stimulation of the digits by the motorized tactile stimulator.

Stimulation protocols. We used two tactile stimulation protocols, protocol 1 and protocol 2, and protocol 2 is the focus of this study. Both protocols used the same motorized, computer-controlled stimulator that could position and indent a bar at arbitrary orientations and locations on the restrained hand. In protocol 1, the stimulator indented a small oriented bar (Ultem plastic) onto the center of the distal, middle, and proximal finger pads of digits two through five (of the hand contralateral to the recorded hemisphere). Stimuli were presented in a pseudorandom order to minimize the time spent traveling between finger pads. After stimulating a pad with a random sequence of two repetitions of each of the eight orientations (22.5° increments), the bar was moved to a randomly chosen neighboring finger pad. This sequence was repeated until each pad had been presented with eight repetitions of each of the eight orientations. Stimulus duration was 500 ms, with an indentation force of 10 g. The bar was approximately the width of a monkey’s finger and had rounded ends; its short axis was a 90° wedge, and its long axis was circular with an 8 mm radius, effectively producing a length of ~7 mm. The responses obtained from this protocol were used to determine the receptive field (RF) size of the neuron and to determine which finger pads were orientation tuned (Fitzgerald et al., 2004, 2006a,b).

Protocol 2 was performed on a single distal finger pad for a neuron that exhibited tuning in the center of that pad during protocol 1. By adjusting the hand holder, the stimulated finger was inclined slightly above the other digits to prevent the oriented bar from touching them. For this protocol, the stimulus bar (Ultem plastic) consisted of a 25-mm-long bar raised on a smooth, flat disk. The ends of the bar and edge of the disk never contacted the finger pad. The short axis of the bar was a 90° wedge, with an apex 500 μm above the disk surface. During each trial, the bar was rotated to one of eight orientations (22.5° increments) and indented into the skin at one of nine positions per orientation (Fig. 1a). The center position of the nine positions per orientation was the center of the finger pad, and the other four positions on either side were spaced in 1 mm increments orthogonal to their orientation, such that the most offset pair of bars was 4 mm from the center of the pad. Thus, the stimuli spanned the contact patch of the finger pad. The bar was indented 1500 μm into the skin (from the point of contact of the apex of the bar), with a 500 ms period of steady indentation and 50 ms fall and rise times. A 1500 μm indentation was chosen because it allowed the bar to be indented into the uniformly flattened finger pad produced by the disk. The disk produced a slightly elliptically shaped contact patch, whose long axis was aligned with the distal–proximal axis of the finger. The interstimulus interval was 2 s. After stimulating the finger pad with a random sequence of all 72 orientation/position combinations, the stimulator repeated this process four more times (for a total of five samples at each combination), each time moving through all 72 combinations in a different random sequence.

We studied neurons on the four distal pads of D2–D5, with D5d being the smallest of the four pads and the pad that we least frequently studied; its compressed width was ~8 mm and its length was ~10 mm. These dimensions are slightly larger than those of the uncompressed distal pad. We centered the bar at the midpoint between the interphalangeal crease and the distal edge of the pad; the bar was never so proximal as to touch the crease.

Histology. After the recordings were completed, each monkey was deeply anesthetized and perfused transcardially. Electrode tracks, which had been marked with fluorescent dyes (DiCarlo et al., 1996), were re-

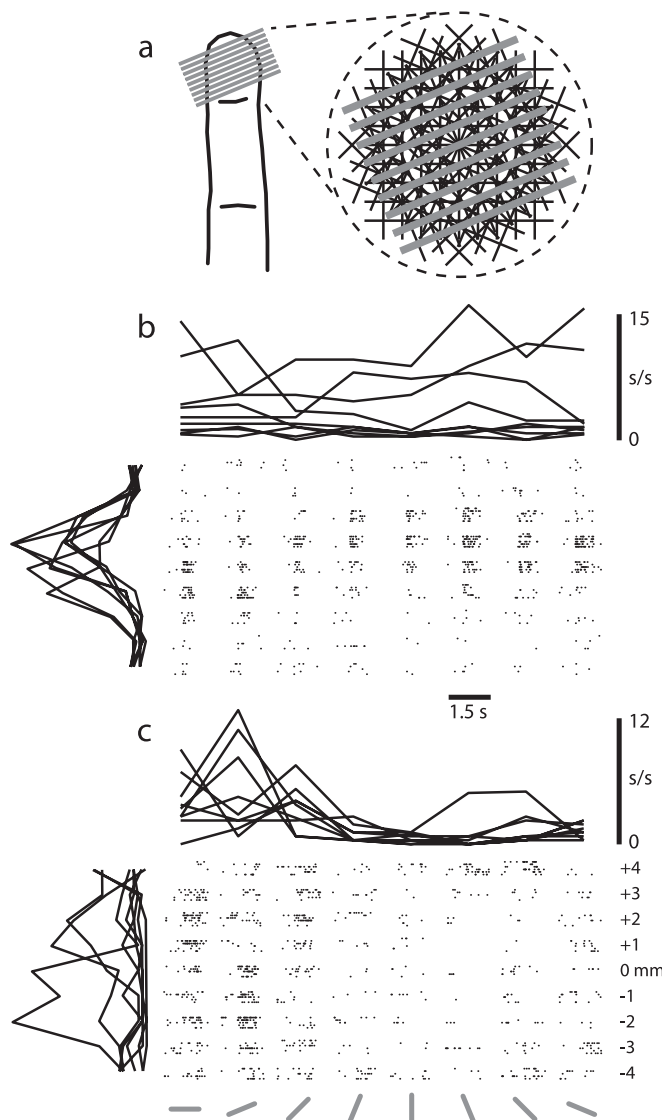


Figure 1. Stimulation protocol and example rasters. **a**, Stimulation protocol, which stimulated a single distal finger pad with an indented oriented bar. We refer to this as protocol 2. For each stimulus presentation (see Materials and Methods), the bar was rotated to one of eight orientations (22.5° increments) and indented into the skin at one of nine positions per orientation. The center position of the nine positions per orientation was centered within the finger pad, and the other four positions on either side were spaced in 1 mm increments orthogonal to their orientation. **b**, Example raster (bottom right), position plots (left), and orientation tuning plots (top) for neuron CJ020_8 that exhibited a divergent vector field that could be explained as a spot of excitation on the distal pad. In the raster, the data are sorted by the eight orientations and nine positions. In the position plots, each curve represents the mean firing rates of one orientation for the nine positions. In the orientation tuning plots, each curve represents the mean firing rates of one position for the eight orientations. **c**, Example raster, position plots, and orientation tuning plots for neuron CJ001_11 that exhibited an invariant vector field and thereby showed position invariant tuning throughout the distal pad. s/s, Spikes per second.

constructed in NeuroLucida and AutoCAD to confirm that the recordings were made in the SII region. We classified each neuron as belonging to the SII region posterior, central, or anterior field based on the subjective multiunit response properties (Fitzgerald et al., 2004).

Data analysis. In a previous study (Fitzgerald et al., 2004), we statistically tested for orientation tuning in the center of the 12 finger pads stimulated during protocol 1. Based on the results from this protocol, we selected the distal finger pad that showed the best tuning for additional study using protocol 2.

Vector fields. For each neuron that was studied using protocol 2, we created a vector field representing the orientation tuning profile of the

F1

AQ: G

AQ: C

finger pad. To do so, the firing rates evoked by the five presentations of the bar at a given orientation (θ) measured with respect to the mediolateral axis in the counterclockwise direction and distance (d) from the center of the finger pad were averaged to obtain a sample of the rate function $r(\theta, d)$ at the particular θ and d . The samples were spline interpolated along the d dimension to a density of $10 \mu\text{m}$ increments to obtain a high-resolution rate function, which was then used to estimate the rates corresponding to the eight orientations at 509,131 points on the finger pad. Specifically, the distance d_θ from the center of the finger pad for a bar oriented at an angle θ and passing through a point $P(x, y)$ is as follows:

$$\begin{aligned} d_\theta &= x \sin \theta - y \cos \theta & \text{for } 0 < \theta < \pi, \\ d_\theta &= y & \text{for } \theta = 0. \end{aligned}$$

Thus, for each of the eight bar orientations, the corresponding distance d_θ was computed at each point $P(x, y)$ using the above equation, and the rates corresponding to the eight orientations at the point $P(x, y)$ were obtained from $r(\theta, d)$.

A vector field was then constructed to quantify the local tuning throughout the pad. A vector $V(x, y)$ was calculated at each point $P(x, y)$, having a magnitude equal to one minus the circular variance (CV) (Fisher, 1993) at that point and a direction equal to the preferred orientation. The circular variance and phase angle of $V(x, y)$ are, respectively, as follows:

$$\begin{aligned} \text{CV} &= 1 - \frac{\left| \sum_{\theta=0}^{7\pi/8} r_\theta e^{2i\theta} \right|}{\sum_{\theta=0}^{7\pi/8} r_\theta} \\ \alpha &= \frac{1}{2} \tan^{-1} \frac{\sum_{\theta=0}^{7\pi/8} r_\theta \sin(2\theta)}{\sum_{\theta=0}^{7\pi/8} r_\theta \cos(2\theta)}, \end{aligned}$$

where r_θ is the rate corresponding to orientation (θ) at the point $P(x, y)$.

AQ: D

Next, we estimated how well the vector field of each neuron matched each of three theoretical vector fields on the finger pad: an invariant (I) field, a divergent (D) field, and a curled (C) field (see supplemental data, available at www.jneurosci.org as supplemental material). The invariant field has all vectors pointing in the same direction and provides a direct measure of position invariant orientation tuning. The divergent field has vectors radiating from an untuned subregion and indicates that a neuron has higher firing rates in this subregion than in the surround. The simplest divergent RF structure is a spot of excitation in the subregion, which “attracts” the vectors. As such, bars placed at the center of the subregion will produce high firing rates but no orientation tuning, and bars centered outside the subregion but which touch it will also elicit high firing rates.

The curled field has vectors that are tangential to an untuned central subregion, and this indicates that a neuron has lower firing rates when the bar is placed in this subregion than in the surround. The simplest curled RF structure is a spot of inhibition in the subregion, which “repels” the vectors. Thus, bars placed at the center of the subregion will produce low firing rates and no orientation tuning, and bars centered outside the subregion but which touch it will also elicit low firing rates.

We performed a least-squares fit to obtain the best fitting version of each of these three theoretical vector fields for a given neuron. The angle between the vector field of the neuron and each of the three best fitting theoretical vector fields, treating each field as a single vector in a higher dimensional space (a vector field spanning N points can be treated as a single vector in $2N$ -dimensional space), is a measure of the goodness of fit. This angle, which we call the proximity measure, was computed by taking the inverse cosine of the Frobenius norm of the best fitting theo-

retical vector field divided by the Frobenius norm of the observed vector field of the neuron. Significance of the fit was determined by resampling (with replacement) the rates at each orientation and distance from the center of the pad and repeating the analysis 500 times to obtain a distribution of the proximity measures. A field was considered purely invariant (I) only if the proximity measure to an invariant field was lower than the proximity measure to a divergent or curled field and the overlap between the distributions of proximity measures to an invariant field and proximity measures to divergent and curled fields was not significant ($p > 0.05$). If the distribution had a significant overlap with the distribution of one of the other test fields, the field was considered mixed (ID, IC, or DC). If there was significant overlap between all of the distributions of the proximity measures for the three fields, the field was termed heterogeneous (H).

Proximity measure. Let $V \in C_{n \times n}$ be the observed vector field. (Here C is a complex vector field of dimensions $n \times n$.) The matrix V can be written in terms of its real and imaginary components as follows:

$$V = V_R + iV_i.$$

The vector field V can also be split into two mutually orthogonal components, I_θ and $I_{\theta + \pi/2}$, such that I_θ is composed of vectors oriented along θ , and $I_{\theta + \pi/2}$ is composed of vectors oriented along $\theta + \pi/2$. Thus, we have for $\forall x, y \in [1, n]$,

$$I_\theta(x, y) = [V_R(x, y)\cos\theta + V_I(x, y)\sin\theta](\cos\theta + i\sin\theta)$$

$$I_{\theta + \pi/2}(x, y) = [-V_R(x, y)\sin\theta + V_I(x, y)\cos\theta](i\cos\theta - \sin\theta)$$

Thus, $V = I_\theta$ and $I_{\theta + \pi/2}$.

Taking the l_2 norm,

$$\begin{aligned} \|I_\theta\|^2 + \|I_{\theta + \pi/2}\|^2 &= \sum_{x, y=1}^n |I_\theta(x, y)|^2 + \sum_{x, y=1}^n |I_{\theta + \pi/2}(x, y)|^2 \\ &= \sum_{x, y=1}^n [V_R(x, y)\cos\theta + V_I(x, y)\sin\theta]^2 \\ &\quad + [-V_R(x, y)\sin\theta + V_I(x, y)\cos\theta]^2 \\ &= \sum_{x, y=1}^n V_R(x, y)^2 + V_I(x, y)^2 \\ &= \|V\|^2. \end{aligned}$$

Thus, this system can be represented as a right triangle, with the length of the hypotenuse equaling $\|V\|$ and the length of the other two sides equaling $\|I_\theta\|$ and $\|I_{\theta + \pi/2}\|$, respectively. The angle between the hypotenuse and the side equaling $\|I_\theta\|$, given as $\alpha = \cos^{-1} \frac{\|I_\theta\|}{\|V\|}$, is a measure of how close the observed vector field is to an invariant field oriented at θ , where θ is chosen such that $I_{\theta + \pi/2}$ is minimized, which in turn minimizes α . If a vector field is untuned, then the vectors will project randomly in every direction, and the distribution of the angles of vectors for the vector field will be uniform and the probability of a vector projecting in any direction will be equal. In other words, $\|I_\theta\| = \text{constant for } \forall \theta \in [0, \pi]$, $\|I_\theta\| = \|I_{\theta + \pi/2}\|$, and $\alpha = 45^\circ$. For an invariant vector field, when $I_{\theta + \pi/2}$ is minimized, $\|I_\theta\| = \|V\|$, and $\alpha = 0^\circ$. As the vector field varies from being invariant to random, α will vary from 0° to 45° .

Proximity to divergent and curled fields. Instead of splitting the vector field into I_θ and $I_{\theta + \pi/2}$, the vector field V can also be split into a divergent

field D_{x_c, y_c} , and a curled field C_{x_c, y_c} , with their centers located at (x_c, y_c) . Thus, we have for $\forall x, y \in [1, n]$:

$$D_{x_c, y_c}(x, y) = \left[V_R(x, y) \cos \left[\tan^{-1} \left(\frac{y - y_c}{x - x_c} \right) \right] + V_I(x, y) \sin \left[\tan^{-1} \left(\frac{y - y_c}{x - x_c} \right) \right] \right] \left(\cos \left[\tan^{-1} \left(\frac{y - y_c}{x - x_c} \right) \right] + i \sin \left[\tan^{-1} \left(\frac{y - y_c}{x - x_c} \right) \right] \right)$$

and

$$C_{x_c, y_c}(x, y) = \left[-V_R(x, y) \sin \left[\tan^{-1} \left(\frac{y - y_c}{x - x_c} \right) \right] + V_I(x, y) \cos \left[\tan^{-1} \left(\frac{y - y_c}{x - x_c} \right) \right] \right] \left(-\sin \left[\tan^{-1} \left(\frac{y - y_c}{x - x_c} \right) \right] + i \cos \left[\tan^{-1} \left(\frac{y - y_c}{x - x_c} \right) \right] \right)$$

Thus,

$$V = D_{x_c, y_c} + C_{x_c, y_c}$$

Also,

$$\|V\|^2 = \|D_{x_c, y_c}\|^2 + \|C_{x_c, y_c}\|^2$$

In this case, $\alpha = \cos^{-1} \frac{\|D_{x_c, y_c}\|}{\|V\|}$ measures the proximity of the observed vector field to a divergent vector field with center located at (x_c, y_c) . A measure of 0° implies a perfectly divergent field centered around (x_c, y_c) , whereas a measure of 45° implies no divergence. The position (x_c, y_c) is chosen such that $\|C_{x_c, y_c}\|^2$ is minimized, thus maximizing α . Similarly, a measure of the proximity of the observed vector field to a curled vector field can be obtained by $\beta = \cos^{-1} \frac{\|C_{x_c, y_c}\|}{\|V\|}$. In this case, $\|D_{x_c, y_c}\|^2$ is minimized by varying (x_c, y_c) . A measure of 0° implies a perfectly curled field centered around (x_c, y_c) , whereas a measure of 45° implies no curling.

Linear receptive fields. We also used a linear regression model (DiCarlo et al., 1998) to obtain linear RFs (see Figs. 2, 3) that best explain the observed responses to the oriented bar in protocol 2. Specifically, we defined a 21×21 (8×8 mm) pixel grid of the distal finger pad, in which each pixel ($400 \mu\text{m}$ square) had an associated weight (w) that defined the effect (excitatory if positive, inhibitory if negative) of that region on the overall firing rate of the neuron. Because we stimulated the finger pad at eight orientations and nine positions per orientation centered on the pad (Fig. 1a), a central, 16-sided polygonal region of the pad was equally stimulated during the protocol, whereas the edges of the pad were stimulated with fewer orientations/positions. Therefore, we only included a central region of 329 pixels in the regression analysis. For a particular bar stimulus presentation, pixels that were stimulated were assigned a value of one ($S = 1$), and all other pixels were assigned a value of zero ($S = 0$). The rate predicted by the regression model can be written as follows:

$$\hat{r}_j = w_0 + \sum_{i=1}^{329} w_i S_{i,j}$$

We used spline interpolation to infer the mean rates, obtained from the eight orientations (22.5° increments) and nine positions (1 mm spacings) per orientation, to a density of 24 orientations (7.5° increments) and 801 positions ($10 \mu\text{m}$ spacings) per orientation, thus yielding a system of 19,224 equations (24 orientations \times 801 positions) in 329 variables. The linear RF was then the least-squares solution to this system of equations. Note that we explicitly inverted the stimulus matrix, and, as such, the RF that we computed accounts for stimulus autocorrelation.

Significance of each weight was determined using a bootstrap analysis. For each position and orientation, the rates were resampled with replacement, spline interpolated, and subjected to the regression analysis 400 times. The weight of a given pixel was considered significant if it had the same sign (excitatory or inhibitory) on $>95\%$ (380 of 400) of the iterations.

Goodness of fit was determined using R^2 , which was computed using the following equation:

$$R^2 = \sum_j \frac{(\hat{r}_j - \bar{r})}{(r_j - \bar{r})}$$

where \hat{r}_j is the rate predicted by the regression model at the j th stimulus presentation, and \bar{r} is the mean rate over all the stimulus presentations (24×801). Regression analysis at a number of different levels of interpolation of the rate function yielded similar results.

R^2 is a measure of the fraction of the total variability that can be attributed to a linear component in the neural response to the oriented bar. The remaining variability corresponds to variability in the neural response (noise) and to the nonlinear component of the neural response.

Nonlinearity. Matching pursuit regression with an overcomplete dictionary of kernels was used to capture different types of nonlinearity in the neural responses (Friedman and Stuetzle, 1981; Mallat and Zhang, 1993). We defined three classes of kernels. The first class, C_α , corresponded to linear weights for each of the 329 pixels (similar to the linear RFs described above). The second class, C_β , contained 24 weights for the 24 orientations. The third class, C_γ , had 24×329 weights, each corresponding to a particular orientation in a pixel. Thus, C_α captures the local tuning aspect of the response, whereas C_β captures the position invariant tuning aspect of the response. The three classes together represent an overcomplete dictionary of kernels, and, hence, any observed response can be completely explained by this set of kernels. We used an iterative regression method, in which the best fitting kernel was selected at every step. At the end of each iteration, the current rate vector was replaced by the residual component by subtracting the projection along the selected kernel. This ensures that the algorithm at the next iteration attempts to capture the component of the rate vector not already accounted for by the kernels selected up to the current iteration. The regression was computed over a response set that was spline interpolated to a density of 24 orientations and 801 positions, as in the case of linear regression mentioned above. However, unlike in the linear regression, the spline interpolation here was performed over individual samples instead of the mean response at every orientation and position. This yielded five samples of the rate at every orientation and position, which was used to compute the residual sum of squares. This was necessary to terminate the iterative regression before the kernels started capturing variability attributable to intertrial fluctuations. At the end of each iteration, a regression sum of squares was computed and compared with the error sum of squares after correcting for the residual sum of squares. The regression was terminated when the addition of another kernel did not yield a significant improvement in the fit (partial F test, $p > 0.05$). Typically, the first 200–300 kernels captured $>95\%$ of the variability of the response.

If $w_i(C)$ is the i th kernel from class C , and $S_{j,i}(C)$ is the projection (1 or 0) of stimulus j on the i th kernel from the class, then the predicted response for the j th stimulus is as follows:

$$\hat{r}_j = w_0 + \sum_i w_i(C_\alpha) S_{j,i}(C_\alpha) + \sum_i w_i(C_\beta) S_{j,i}(C_\beta) + \sum_i w_i(C_\gamma) S_{j,i}(C_\gamma)$$

We defined the predicted response that was accounted for by each class, by regressing the responses against the kernels from that class. Let $\hat{r}_j(C_\alpha)$ and $\hat{r}_j(C_\beta)$ be the predicted responses accounted for by the linear and invariant classes, respectively. We then quantified the linearity and position invariant tuning of a neuron by the fraction of variability explained

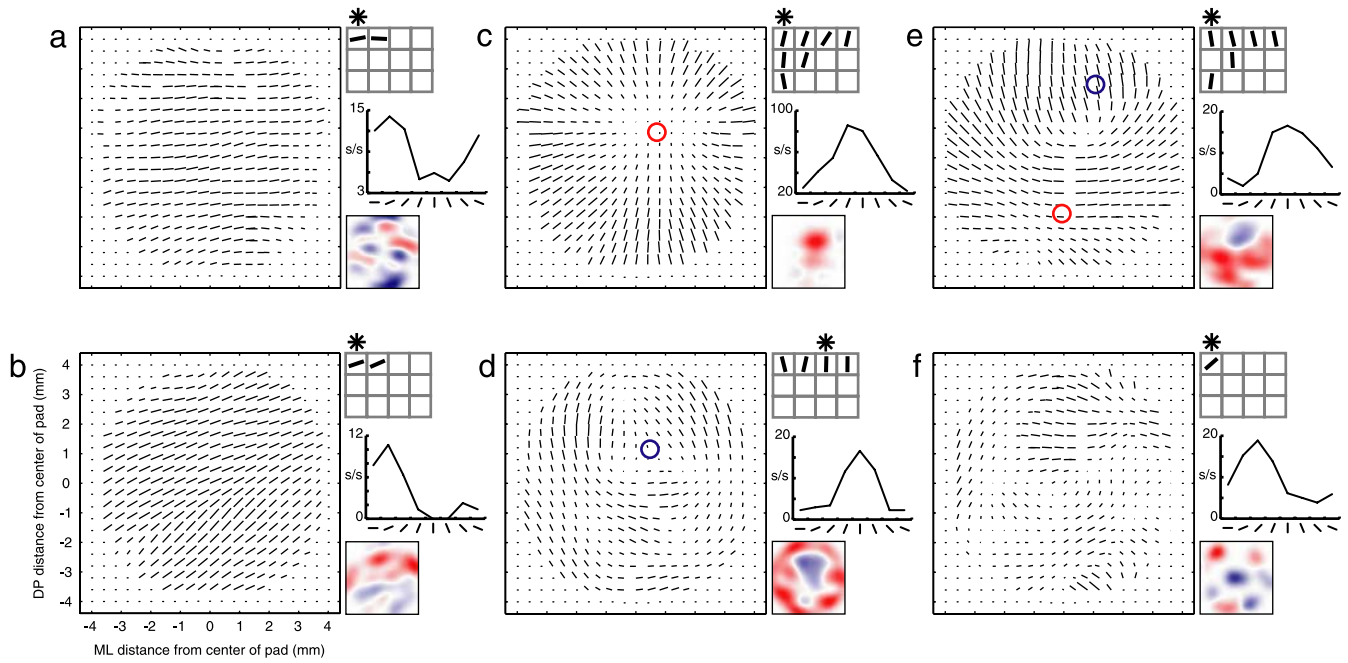


Figure 2. Example vector fields. **a**, Data from neuron CK00P_6, which exhibited an invariant vector field (left), with mean preferred orientation of 7.4°. Within the vector field, each short line segment is a vector that represents the preferred orientation (direction) and strength (magnitude) of tuning at that point on the distal finger pad. Red circles indicate the center of divergence, whereas blue circles indicate the center of curling. Also shown is the preferred orientation diagram (top right) from protocol 1, the orientation tuning curve (middle right) from protocol 1 of the pad stimulated during protocol 2, and the linear receptive field (bottom right) from protocol 2. In the preferred orientation diagram (top right), the gray 3 × 4 grid represents the 12 finger pads of D2–D5, with the top row of the grid representing the distal pads and the left column representing D2. The black line segments within the grid represent the mean angular vector (preferred orientation) of the tuned finger pads, and the asterisk indicates the distal pad studied during protocol 2. In the orientation tuning plot (middle right), each of the eight points in the curve represents the mean firing rate during the 500 ms presentation of the particular orientation. In the linear receptive field (bottom right), redness represents excitation and blueness represents inhibition, and the degree of redness or blueness is proportional to the magnitude of excitation or inhibition, respectively. **b**, Neuron CJ020_8 (Fig. 1*b*) exhibited a divergent vector field, centered, relative to the center of the finger pad, at mediolateral (ML) 0.73 mm and distal-proximal (DP) 0.86 mm. **c**, Neuron CJ001_11 (Fig. 1*c*) also exhibited an invariant vector field (mean preferred orientation of 29.7°). **d**, Neuron CM01C_6 exhibited a curled vector field, centered at ML 0.46 mm and DP 1.27 mm. **e**, Neuron CL014_4 exhibited a mixed (DC) vector field, with divergence centered at ML –0.13 mm and DP –1.87 mm and curling centered at ML 1.11 mm and DP 2.67 mm. **f**, Neuron CL011_8 exhibited a heterogeneous vector field.

by the kernels from the first two classes, respectively, using the following equations:

$$R_{lin}^2 = \sum_j \frac{(\hat{r}_j(C_\alpha) - \bar{r})}{(r_j - \bar{r})}$$

$$R_{inv}^2 = \sum_j \frac{(\hat{r}_j(C_\beta) - \bar{r})}{(r_j - \bar{r})}$$

R_{lin}^2 and R_{inv}^2 quantify, on a scale of 0–1, the degree to which the purely linear model and the purely invariant model explain the data compared with a null model consisting of a uniform response. We defined another quantity, R_{local}^2 , to quantify the fraction of the response that was explained by the local tuning kernels,

$$R_{local}^2 = \sum_j \frac{(\hat{r}_j - \hat{r}_j(C_\alpha, C_\beta))}{(r_j - \hat{r}_j(C_\alpha, C_\beta))}$$

Here $\hat{r}_j(C_\alpha, C_\beta)$ is the rate predicted by a composite model of linear and invariant weights and is obtained by regressing the response against both the linear and invariant class kernels.

Results

Vector fields

Figure 1, *b* and *c*, shows raster plots of the responses of two example neurons to bars placed at multiple orientations and locations on the distal finger pad. Although both of these neurons showed orientation-tuned responses when the bar was centered on the finger pad (Fig. 2*b,c*), the responses to the bar varied greatly for each neuron depending on how the bar was presented

to the finger pad. For example, the neuron shown in Figure 1*b* responded well to the bar when it was placed within the central 4 mm of the pad. However, its responsiveness dropped off dramatically as the bar was positioned toward the edges of the pad. We show later that neurons of this type had simple cell-like RF structures with distinct regions of excitation and inhibition.

In contrast, many other neurons in the SII region showed position invariant responses, and one such neuron is shown in Figure 1*c*. This neuron responded well to horizontal bars and poorly to vertical bars, independent of where the bar was placed on the finger pad. These results suggest that the orientation selectivity of different neurons in the SII region is based on different underlying mechanisms.

To quantify the tuning characteristics of the neurons, we computed two-dimensional vector fields that estimated the local orientation tuning at >500,000 locations on the finger pad (see Materials and Methods). We then used a proximity measure to determine whether different regions of the vector fields fell into one of three types, which we called invariant (I), divergent (D), and curled (C). Type I were regions in which all of the vectors tended to point in the same direction, indicating position invariant orientation tuning.

Type D were regions in which the vectors radiate from a central untuned subregion. This radiating pattern of vectors is most easily explained by an excitatory or “hot” spot comprising the untuned subregion that produced higher firing rates when part of the bar contacted the hot spot and therefore “attracted” the vectors (see supplemental data, available at www.jneurosci.org as

supplemental material). However, a divergent field could theoretically arise from any RF in which a central subregion is more responsive than its surround. In particular, the central subregion could be excitatory, unresponsive, or even inhibitory, as long as the surrounding region is less responsive (i.e., has a lower evoked firing rate).

Type C were regions in which the vectors point tangentially to a central untuned subregion. This curled pattern of vectors is most easily explained by an inhibitory or “cold” spot in the untuned subregion that produced lower firing rates when in contact with the bar, and therefore “repelled” the vectors. However, a curled field could theoretically arise from any RF in which a central subregion is less responsive than its surround. In particular, the central subregion could be inhibitory, unresponsive, or even excitatory, as long as the surrounding region is more responsive (i.e., has a higher evoked firing rate).

Example vector fields for six SII region neurons are shown in Figure 2. We encountered neurons that had purely I fields, a single D field, or single C field, combinations of these that we called ID, IC, and DC, as well as H vector fields that could not easily be explained by one or more of these vector field types. Examples of two neurons that were purely I across the entire finger pad are shown in Figure 2, *a* and *b*. For these neurons, the individual vectors point in the same direction throughout the pad, although the magnitudes of the vectors and thus the strength of tuning vary somewhat across the pad. Other purely invariant neurons exhibited a similar preferred orientation throughout most of the pad, whereas the tuning was very weak or nonexistent throughout the rest of the pad. Fifteen of the 61 neurons had purely invariant vector fields. The proportions of invariant neurons in the three SII region fields were as follows: posterior field, 1 of 4; central field, 12 of 40; and anterior field, 2 of 17. These proportions are not significantly different (exact test, $p > 0.05$).

Figure 2, *c* and *d*, shows examples of neurons with a single D and single C field, respectively. Inspection of Figure 2*c* indicates that the individual vectors point toward a small untuned subregion that was displaced slightly distal and medial to the center of the pad. Eleven of the 61 neurons had simple divergent vector fields. The proportions of divergent neurons in the three SII region fields were as follows: posterior field, 0 of 4; central field, 8 of 40; anterior field, 3 of 17. These proportions are not significantly different (exact test, $p > 0.05$). Only six of the 61 neurons had simple curled vector fields like the one shown in Figure 2*d*. For these neurons, the vectors pointed tangential to and curled about the untuned subregion, which for the example neuron is slightly distal to the center of the pad. Five of the six neurons of this type were found in the central field, although the proportions in the three SII region fields were not significantly different (exact test, $p > 0.05$).

The vector fields of many SII region neurons did not fall cleanly into one of the above basic vector field types in that the fields were matched well by two of the three field types (ID, IC, or DC) or instead were heterogeneous. Figure 2*e* shows a neuron that was categorized as DC. Vectors in the top right tend to curl about a subregion, whereas vectors near the center bottom tend to radiate outward from another subregion. Five of the 61 neurons were categorized as DC, and five others were categorized as either ID or IC. A total of 20 of 61 or 33% of the sample of tuned SII region neurons (including 15 purely I neurons) exhibited some degree of position invariance.

For the neurons shown in Figure 2, *d* and *e*, there are discrepancies between the tuning observed at the center of the finger pad for protocol 1 and protocol 2. We think two factors may be con-

Table 1. The goodness of fit of the linear model

Type	<i>n</i>	Linear r^2	SD
I	15 (24.6%)	0.43	0.16
D	11 (18.0%)	0.60	0.11
C	6 (9.8%)	0.49	0.07
ID	2 (3.3%)	0.65	0.02
IC	3 (4.9%)	0.51	0.12
DC	5 (8.2%)	0.64	0.11
H	19 (31.1%)	0.48	0.10
Totals	61	0.51	0.13

Type, Vector field type; *n*, number of neurons.

tributing to these differences: (1) slight differences in the placement of the two bars and (2) differences in the shapes of the two bars. Factor 1 is relevant because we had to manually incline the finger after protocol 1 to study that finger during protocol 2. In doing so, we re-centered the bar on the finger pad by eye, which probably resulted in a slightly different centering of the bar in the two protocols. Factor 2 may also have contributed to the discrepancies in tuning, because the bar in protocol 2 was much longer and embossed on a flat disk. Indeed, inspection of the vector fields in Figure 2, *d* and *e*, indicates that tiny differences in the location of the bar would produce substantially different tuning, and, with the large differences between the shapes of the two bars, it is not surprising that for some of the neurons there is a discrepancy in the tuning at the center of the pad for the two protocols.

Figure 2*f* shows data from a neuron that had a vector field that was categorized as heterogeneous. Neurons in this group had vector fields that tended to be highly complex, with mixed regions of tuned and untuned vectors that were not systematically organized into a single divergent, curled, or invariant field. The proportions of heterogeneous neurons in the three SII region fields were as follows: posterior field, 2 of 4; central field, 12 of 40; anterior field, 5 of 17. These proportions are not significantly different (exact test, $p > 0.05$).

Linear receptive fields

The responses to the oriented bars were also used to compute a linear RF for each of the 61 neurons (see Materials and Methods). The mean goodness of fit of the model was reasonably high for all of the neurons (Table 1). Although the mean was lower for the 20 neurons with invariant vector fields (I, ID, and IC; mean of 0.46) than for the 41 non-invariant neurons (D, C, DC, and H; mean of 0.53), the difference was not significant (two-tailed *t* test, $p > 0.05$). Figure 3 shows the linear RFs for all 61 neurons. Visual inspection of these linear RFs clearly indicates that, across all neuron types, SII region RFs do not have uniform regions of excitation or inhibition but in general are asymmetric with multiple regions of excitation and inhibition.

Purely I neurons contained a variety of different structures within their linear RFs, indicating that there is no simple characteristic pattern that explains these responses. In addition, for these neurons, there is no clear relationship between the vector fields and the linear RFs (Fig. 2*a,b*). Purely D neurons tended to have either a single dominant region of excitation (for examples, see Fig. 3, b3 and b4) or a dominant region of excitation among several other regions of significant excitation or inhibition (for example, see Fig. 3, d4), and, as such, the vector fields are explained well by these linear RFs (Fig. 2*c*). C neurons tended to have a center-surround organization (Fig. 2*d*), with inhibition in the center of the pad and excitation near the edges of the pad. Mixed (ID, IC, and DC) neurons also appeared to have single or

AQ: E

F3

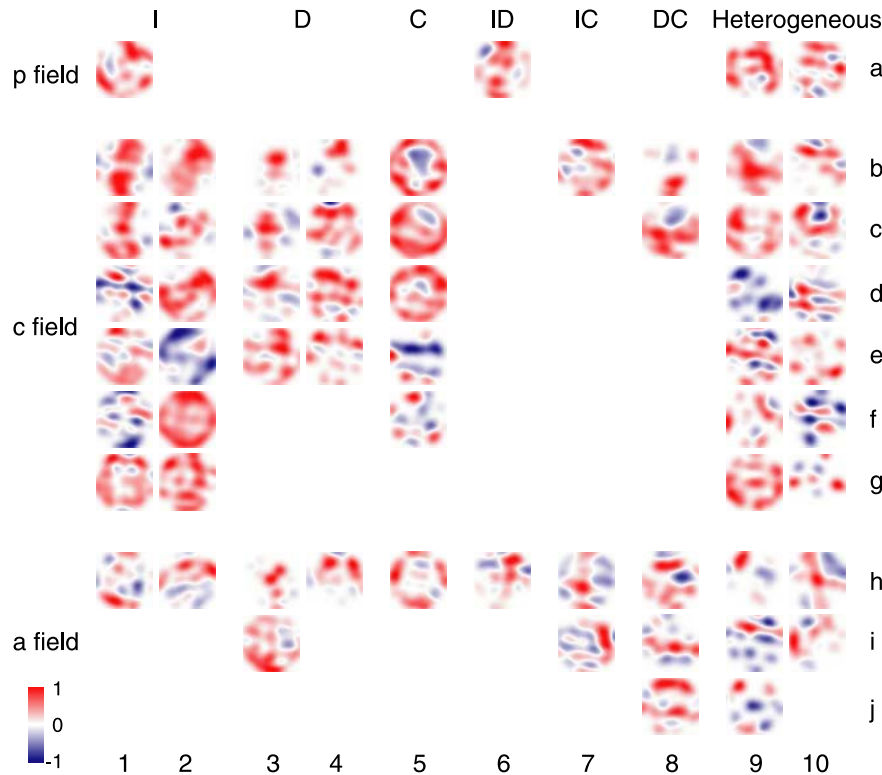


Figure 3. Linear receptive fields. Each linear field represents the stimulated distal finger pad for a single neuron. Red areas denote excitation, blue areas denote inhibition, and white areas denote no significant driving. The intensity of the red or blue areas is proportional to the magnitude of excitation or inhibition, respectively. The neurons are arranged according to SII region field (p, posterior; c, central; a, anterior) and vector field category (I, invariant; D, divergent; C, curled; ID, IC, DC, mixed; H, heterogeneous). Within each SII region field and vector field category, the receptive fields are sorted from highest goodness of fit (top) to lowest goodness of fit (bottom). Linear fields for the example neurons shown in Figures 1 and 2: CJ020_8, b3; CJ001_11, h2; CK00P_6, f1; CM01C_6, b5; CL014_4, c8; and CL011_8, j9.

dominant regions of excitation or inhibition, although perhaps surprisingly each ID neuron contained significant inhibition, and each IC neuron contained significant excitation. H neurons contained a variety of excitatory and inhibitory subregions within their linear RFs, consistent with these neurons showing complicated vector fields, although their linear RFs were not necessarily more complicated than those of the other neuron types.

An inspection of the RFs shown in Figure 3 suggests that few of the RFs have simple explanations for orientation tuning, although a few neurons appear to contain a single oriented band of excitation or inhibition traversing the center of the finger pad (examples b1 and i8); therefore, tuning for many neurons probably arose from other asymmetries in the RF, and, in some cases, this may not be accounted for by the linear RFs. Many of the linear RFs had multiple bands of excitation and/or inhibition that were typically close to horizontal (examples d4, a10, and d10), and many other RFs had multiple patches of excitation and/or inhibition (examples f1 and f10). Finally, there was no significant difference in the mean linear goodness of fit between the three SII region fields (means: p field, 0.52; c field, 0.50; a field, 0.53; one-way ANOVA, $p > 0.05$), and visual comparison of the linear RFs between the three SII fields suggests that the RFs are similar.

Analysis of nonlinearity

The data were further analyzed using a modified matching-pursuit algorithm to determine the degree to which the responses were captured by nonlinear position invariant mechanisms and by linear mechanisms (see Materials and Methods). We found

that the responses of neurons with simple vector fields (D, C, and DC) were captured well by linear kernels and that neurons with purely I responses had greater degrees of nonlinearity. This is shown in Figure 4, in which purely invariant neurons tended to cluster farther to the right (higher invariance r^2) and down (lower linear r^2) than most non-invariant neurons. Neurons with mixed invariant vector fields (ID and IC) lie midway between the two groups. The responses of H neurons (data not shown) showed lower linear r^2 values than neurons with simple vector fields, although they also showed lower invariance r^2 values than I neurons. Overall, the mean r^2 for the invariance measure was significantly higher for the 20 invariant (I, ID, and IC) neurons (means of linear, invariance, and local: 0.45, 0.22, and 0.33) than for the 41 non-invariant neurons (means: 0.50, 0.11, and 0.37), although there was no significant difference for the linear and local measures (three separate two-tailed t tests, $p < 0.002$ for invariance measure). There was no significant difference in the mean r^2 between the three SII region fields for the three kernel types (means of linear, invariance, and local: p field, 0.50, 0.13, and 0.35; c field, 0.49, 0.16, and 0.34; a field, 0.48, 0.12, and 0.40; three separate one-way ANOVAs, each $p > 0.05$).

Discussion

The principal finding is that tuning to an oriented bar indented into the center of a finger pad can arise from a variety of mechanisms. Here we show that the tuning can be attributable to a region showing pure position invariance, excitatory and inhibitory spots that are not centered on the pad, bands of excitation or inhibition, or combinations of these types. Neurons that we classified as D, C, and DC are best explained as having distinct regions of excitation and inhibition and are conceptually similar to simple cells in the visual system, whereas the invariant neurons are similar to complex visual neurons (Hubel and Wiesel, 1968). If the analogy with the visual system holds, then the D, C, and mixed neurons may represent early to intermediate steps in a transformation from simple to complex cells. In this model, neurons that have partially invariant (ID and IC) or strongly locally tuned responses provide feedforward, convergent input to neurons that show invariance across the entire finger pad. Another possibility, which is not mutually exclusive, is that the convergent inputs for all of the tuned SII region neurons come from lower-order somatosensory neurons in SI that project to the SII region (Friedman et al., 1980, 1986; Pons et al., 1987, 1992; Burton et al., 1995; Disbrow et al., 2003). Previous studies have shown that many of the RFs in SI show approximately linear response properties and have approximately circular or slightly elongated lobes of excitation or inhibition, like most of the D, C, and DC neurons we report here (DiCarlo et al., 1998; Sripathi et al., 2006). Furthermore, Hyvärinen and Poranen (1978) reported that a few neurons in area 2 showed invariant responses to bars placed at different locations on the hand, indicating that some of

F4

AQ:F

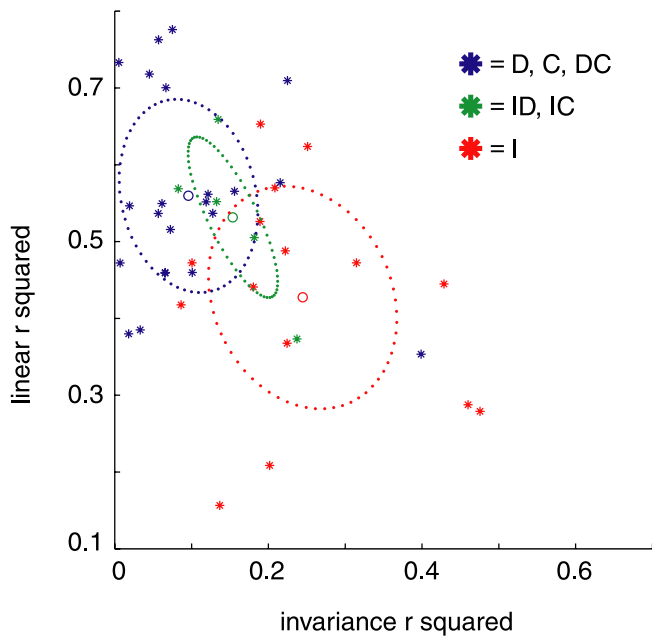


Figure 4. Linear and nonlinear quantification of the neurons. Each color represents neurons from one group of vector field categories (D, C, DC, non-invariant; ID, IC, partially invariant; I, purely invariant), and each small asterisk represents one neuron. The ordinate represents the linear r^2 value of a neuron (first class of kernels; see Materials and Methods), the abscissa represents the position invariance r^2 value (second class of kernels), and the local tuning r^2 value (third class of kernels) is approximately one minus the first two classes of kernels. The colored, open circles represent the mean linear r^2 and invariance r^2 values for each group of vector field categories. The orientation of the major and minor axis of each colored ellipse, for each group of vector field categories, corresponds to the eigenvectors of the covariance matrix of the data points. The length of each axis of the ellipse corresponds to 2 SD in Mahalanobis units, which is twice the square root of the eigenvalues.

AQ: H

the invariant properties of SII region neurons may originate from area 2 neurons.

Orientation versus hot and cold spot tuning

An alternative hypothesis to the hierarchical model described above is that the D, C, and DC neurons are not involved in orientation tuning at all, although this is probably less likely the case for invariant neurons. Instead, perhaps hot and cold spot neurons are involved in detecting other tactile features of the stimuli. For example, neurons that were classified as DC would be prime candidates for extracting information about the spatial variation of surfaces and as such could be involved in coding surface roughness (Johnson et al., 2002), and D and C neurons could play similar roles in coding information about local surface curvature.

The finding that a number of neurons had heterogeneous RF structures that could not be easily explained by one of the three vector field types also suggests that some neurons in the SII region are involved in processing other aspects of the stimulus besides orientation. These neurons had multiple spots of excitation or inhibition (Fig. 3) and possibly multiple patches of invariance (Fig. 2f), each with a different preferred orientation. One hypothesis is that these neurons are selective to complex surface features such as curves and corners.

SII region neurons may exhibit receptive field modularity

In a previous paper (Fitzgerald et al., 2006a), we showed that SII region neurons with multiple tuned pads tend to have similar tuning (i.e., a similar preferred orientation) across multiple finger pads (Fig. 2). Moreover, another study in our laboratory (Na-

kama, 2003) has shown that, for some SII region neurons, the similarity of tuning can include digits on both hands, because many SII region neurons have bilateral RFs (Whitsel et al., 1969; Robinson and Burton, 1980). In the current study, we only examined position invariance within a single, tuned distal finger pad. Therefore, it is not clear whether neurons with multiple tuned pads, many of which have similar tuning at least in the centers of those tuned pads, have similar RF structures comprising each of their tuned pads. A parsimonious hypothesis at this point is that there is a similar RF structure comprising each tuned finger pad of these large RFs and that the RF structures that we report here are repeated on each tuned finger pad of both hands. This suggests that some SII region neurons (type I) exhibit position invariant tuning across large parts of the hand, whereas others (types D, C, and DC) exhibit repeating patterns of excitation and/or inhibition across each of the tuned pads, and, in both cases, this can be thought of as a type of RF modularity. Repeating the same RF patterns across pads, for non-I neurons, is a different kind of position invariance in which the invariance is relative to the local RF structure on the finger pad. The results indicate that SII region neurons are important in processing both the spatial form of small stimuli contacting a single finger pad and the shape of large objects that contact multiple fingers and finger pads.

Position invariant orientation tuning

We showed that the responses of neurons with simple cell-like RFs (D, C, and DC) could generally be explained by the linear RFs shown in Figure 3. Furthermore, we showed that the responses of D, C, and DC neurons were captured well by linear kernels (Fig. 4). However, the responses of position invariant neurons were not explained by the linear RF structures shown in Figure 3. This is to be expected because position invariance suggests that such neurons respond nonlinearly to the stimulus, and, as such, linear RFs showing patterns of excitation and inhibition are a poor way to represent the processing functions of these neurons. In contrast, a significant fraction of the responses of these neurons was captured by the position invariant processing kernels (Fig. 4), illustrating that these neurons are selective to orientation independent of the location of the bar. Such nonlinear responses indicate that these are higher-order neurons involved in tactile shape processing.

The SII region and the somatosensory cortical hierarchy

What do the current data suggest about the posterior, central, and anterior fields, the three representations that comprise the SII region (Fitzgerald et al., 2004)? We studied very few ($n = 4$) neurons in the posterior field and more than twice as many central field neurons ($n = 40$) than anterior field neurons ($n = 17$), primarily because it was more difficult to find tuned neurons in the posterior and anterior fields. Nonetheless, these data suggest that the three fields may have similar proportions of neurons in the various vector field categories and that nearly all of these types of RFs (except for ID in the central field) are represented in both the central and the anterior fields. The structures of the linear RFs from the three fields were also similar, suggesting that the three fields are at a similar hierarchical level. Finally, the finding that position invariance is commonly observed in tuned SII region neurons adds additional support to the hypothesis that the SII region is of higher order than SI.

References

Bincat SL, Connor CE (2004) Underlying principles of visual shape selectivity in posterior inferotemporal cortex. *Nat Neurosci* 7:880–886.

- Burton H, Fabri M, Alloway KD (1995) Cortical areas within the lateral sulcus connected to cutaneous representations in areas 3b and 1: a revised interpretation of the second somatosensory area in macaque monkeys. *J Comp Neurol* 355:539–562.
- Desimone R, Albright TD, Gross CG, Bruce C (1984) Stimulus-selective properties of inferior temporal neurons in the macaque. *J Neurosci* 4:2051–2062.
- DiCarlo JJ, Lane JW, Hsiao SS, Johnson KO (1996) Marking microelectrode penetrations with fluorescent dyes. *J Neurosci Methods* 64:75–81.
- DiCarlo JJ, Johnson KO, Hsiao SS (1998) Structure of receptive fields in area 3b of primary somatosensory cortex in the alert monkey. *J Neurosci* 18:2626–2645.
- Disbrow E, Litinas E, Recanzone GH, Padberg J, Krubitzer L (2003) Cortical connections of the second somatosensory area and the parietal ventral area in macaque monkeys. *J Comp Neurol* 462:382–399.
- Fisher NI (1993) Statistical analysis of circular data. Cambridge, UK: Cambridge UP.
- Fitzgerald PJ, Lane JW, Thakur PH, Hsiao SS (2004) Receptive field properties of the macaque second somatosensory cortex: evidence for multiple functional representations. *J Neurosci* 24:11193–11204.
- Fitzgerald PJ, Lane JW, Thakur PH, Hsiao SS (2006a) Receptive field properties of the macaque second somatosensory cortex: representation of orientation on different finger pads. *J Neurosci* 26:6473–6484.
- Fitzgerald PJ, Lane JW, Thakur PH, Hsiao SS (2006b) Receptive field (RF) properties of the macaque second somatosensory cortex: RF size, shape, and somatotopic organization. *J Neurosci* 26:6485–6495.
- Friedman DP, Jones EG, Burton H (1980) Representation pattern in the second somatic sensory area of the monkey cerebral cortex. *J Comp Neurol* 192:21–41.
- Friedman DP, Murray EA, O'Neill JB, Mishkin M (1986) Cortical connections of the somatosensory fields of the lateral sulcus of macaques: evidence for a corticolimbic pathway for touch. *J Comp Neurol* 252:323–347.
- Friedman JH, Stuetzle W (1981) Projection pursuit regression. *J Am Stat Assoc* 76:817–823.
- Gallant JL, Connor CE, Rakshit S, Lewis JW, Van Essen DC (1996) Neural responses to polar, hyperbolic, and Cartesian gratings in area V4 of the macaque monkey. *J Neurophysiol* 76:2718–2739.
- Graziano MS, Andersen RA, Snowden RJ (1994) Tuning of MST neurons to spiral motions. *J Neurosci* 14:54–67.
- Hubel DH, Wiesel TN (1968) Receptive fields and functional architecture of monkey striate cortex. *J Physiol (Lond)* 195:215–243.
- Hung CP, Kreiman G, Poggio T, DiCarlo JJ (2005) Fast readout of object identity from macaque inferior temporal cortex. *Science* 310:863–866.
- Hyvärinen J, Poranen A (1978) Movement-sensitive and direction and orientation-selective cutaneous receptive fields in the hand area of the post-central gyrus in monkeys. *J Physiol (Lond)* 283:523–537.
- Ito M, Tamura H, Fujita I, Tanaka K (1995) Size and position invariance of neuronal responses in monkey inferotemporal cortex. *J Neurophysiol* 73:218–226.
- Johansson RS, Landstrom U, Lundstrom R (1982) Sensitivity to edges of mechanoreceptive afferent units innervating the glabrous skin of the human hand. *Brain Res* 244:27–35.
- Johnson KO, Phillips JR (1981) Tactile spatial resolution. I. Two-point discrimination, gap detection, grating resolution, and letter recognition. *J Neurophysiol* 46:1177–1191.
- Johnson KO, Hsiao SS, Yoshioka T (2002) Neural coding and the basic law of psychophysics. *The Neuroscientist* 8:111–121.
- Logothetis NK, Pauls J, Poggio T (1995) Shape representation in the inferior temporal cortex of monkeys. *Curr Biol* 5:552–563.
- Mallat S, Zhang Z (1993) Matching pursuit with time-frequency dictionaries. *IEEE Trans Signal Proc* 41:3397–3415.
- Nakama T (2003) System identification analysis of neuronal responses to bimanual stimulation in the second somatosensory cortex. PhD thesis, The Johns Hopkins University.
- Pasupathy A, Connor CE (1999) Responses to contour features in macaque area V4. *J Neurophysiol* 82:2490–2502.
- Phillips JR, Johnson KO, Hsiao SS (1988) Spatial pattern representation and transformation in monkey somatosensory cortex. *Proc Natl Acad Sci USA* 85:1317–1321.
- Pons TP, Garraghty PE, Friedman DP, Mishkin M (1987) Physiological evidence for serial processing in somatosensory cortex. *Science* 237:417–420.
- Pons TP, Garraghty PE, Mishkin M (1992) Serial and parallel processing of tactual information in somatosensory cortex of rhesus monkeys. *J Neurophysiol* 68:518–527.
- Quiroga RQ, Reddy L, Kreiman G, Koch C, Fried I (2005) Invariant visual representation by single neurons in the human brain. *Nature* 435:1102–1107.
- Riesenhuber M, Poggio T (2002) Neural mechanisms of object recognition. *Curr Opin Neurobiol* 12:162–168.
- Robinson CJ, Burton H (1980) Somatotopographic organization in the second somatosensory area of *M. fascicularis*. *J Comp Neurol* 192:43–67.
- Rolls ET (1994) Brain mechanisms for invariant visual recognition and learning. *Behav Processes* 33:113–138.
- Sary G, Vogels R, Orban GA (1993) Cue-invariant shape selectivity of macaque inferior temporal neurons. *Science* 260:995–997.
- Sripati AP, Yoshioka T, Denchev P, Hsiao SS, Johnson KO (2006) Spatio-temporal receptive fields of peripheral afferents and cortical area 3b and 1 neurons in the primate somatosensory system. *J Neurosci* 26:2101–2114.
- Thorell LG, DeValois RL, Albrecht DG (1984) Spatial mapping of monkey V1 cells with pure color and luminance stimuli. *Vision Res* 24:751–769.
- Tovee MJ, Rolls ET, Azzopardi P (1994) Translation invariance in the responses to faces of single neurons in the temporal visual cortical areas of the alert macaque. *J Neurophysiol* 72:1049–1060.
- Wallis G, Rolls ET (1997) A model of invariant object recognition in the visual system. *Prog Neurobiol* 51:167–194.
- Wheat HE, Goodwin AW (2001) Tactile discrimination of edge shape: limits on spatial resolution imposed by parameters of the peripheral neural population. *J Neurosci* 21:7751–7763.
- Whitsel BL, Petrucelli LM, Werner G (1969) Symmetry and connectivity in the map of the body surface in somatosensory area II of primates. *J Neurophysiol* 32:170–183.